Article

Optimized and Far-Red-Emitting Variants of Fluorescent Protein eqFP611

Simone Kredel,[1,9] Karin Nienhaus,[2,9] Franz Oswald,[3,9] Michael Wolff,[1] Sergey Ivanchenko,[2] Florian Cymer,[1] Andreas Jeromin,[4] Francois J. Michel,[5] Klaus-Dieter Spindler,[1] Ralf Heilker,[6] G. Ulrich Nienhaus,[2,7] and Jörg Wiedenmann[1,8,*]

[1]Institute of General Zoology and Endocrinology
[2]Institute of Biophysics
[3]Department of Internal Medicine I
University of Ulm, 89069 Ulm, Germany
[4]Allen Institute for Brain Science, Seattle, WA 98103, USA
[5]Plate-forme d'Imagerie Cellulaire, Institut des Neurosciences, Université Bordeaux II, 33077 Bordeaux, France
[6]Boehringer Ingelheim Pharma GmbH & Co. KG, 88397 Biberach, Germany
[7]Department of Physics, University of Illinois at Urbana-Champaign, Urbana, IL 61801, USA
[8]National Oceanography Centre, University of Southampton, Southampton SO14 3ZH, United Kingdom
[9]These authors contributed equally to this work.
*Correspondence: j.wiedenmann@soton.ac.uk
DOI 10.1016/j.chembiol.2008.02.008

SUMMARY

Fluorescent proteins (FPs) emitting in the far-red region of the spectrum are highly advantageous for whole-body imaging applications because scattering and absorption of long-wavelength light is markedly reduced in tissue. We characterized variants of the red fluorescent protein eqFP611 with bright fluorescence emission shifted up to 639 nm. The additional red shift is caused by a *trans-cis* isomerization of the chromophore. The equilibrium between the *trans* and *cis* conformations is strongly influenced by amino acid residues 143 and 158. Pseudo monomeric tags were obtained by further genetic engineering. For the red chromophores of eqFP611 variants, molar extinction coefficients of up to ~150,000 were determined by an approach that is not affected by the presence of molecules with nonfunctional red chromophores. The bright fluorescence makes the red-shifted eqFP611 variants promising lead structures for the development of near-infrared fluorescent markers. The red fluorescent proteins performed well in cell biological applications, including two-photon imaging.

INTRODUCTION

Imaging of various biological processes in the living cell is a key technology in current biomedical and pharmaceutical research. Arguably, the most important tools in this context are genetically encoded fluorescence markers such as the green fluorescent protein (GFP) from *Aequorea victoria* (Shimomura et al., 1962; Prasher et al., 1992; Chalfie et al., 1994). The discovery of GFP-like proteins from nonbioluminescent anthozoans gave access to a whole array of potential marker proteins, including photoactivatable fluorescent proteins (FPs) (Wiedenmann and Nienhaus, 2006) and the long-sought red fluorescent proteins (RFPs)

(Wiedenmann, 1997; Matz et al., 1999; Fradkov et al., 2000; Lukyanov et al., 2000; Wiedenmann et al., 2000, 2002).

With a few exceptions that form dimers (Ward and Cormier, 1979; Karasawa et al., 2004; Merzlyak et al., 2007), anthozoan GFP-like proteins are obligate tetramers (Wall et al., 2000; Yarbrough et al., 2001; Prescott et al., 2003; Wilmann et al., 2005; Henderson and Remington, 2005; Remington et al., 2005; Nienhaus et al., 2005, 2006a, 2006b). Some species form even higher-order aggregates that have restricted their application and demanded biotechnological optimization (Yanushevich et al., 2002). Tetrameric proteins have been successfully applied as in vivo markers (Terskikh et al., 2000; Wiedenmann et al., 2004; Schiebel and Maekawa, 2004; Janke et al., 2004; Forner and Binder, 2007). However, not all proteins of interest tolerate the oligomerization induced by the tag, and oligomerization may also change characteristic properties of the fusion partner (Campbell et al., 2002). Recently, a number of tandem-dimer and monomeric FP variants have been developed that appear useful for the construction of fusion proteins (Campbell et al., 2002; Karasawa et al., 2003, 2004; Wiedenmann et al., 2004; Shaner et al., 2004; Nienhaus et al., 2006; Merzlyak et al., 2007; Shcherbo et al., 2007; Wang et al., 2004).

It is noteworthy that numerous applications exist that are not sensitive to oligomerization, at least as long as no larger aggregates are formed. Instead, these applications may call for properties such as fast maturation, high brightness, and (photo-)stability of the marker. Examples include studies in which the FP is fused to a short signal peptide to highlight cells or intracellular compartments, for instance mitochondria (Forner and Binder, 2007; Ivanchenko et al., 2007) or peroxisomes (Forner and Binder, 2007). Oligomeric FPs have also been employed successfully in studies of gene activity in cells or tissues (Terskikh et al., 2000). A particularly important application of FPs that is not impeded by the tetrameric nature of the marker is in the area of tissue imaging or whole-body imaging of living model organisms such as mice or frogs, in which they enable, for instance, observations of tumor growth or tracking of metastases (Yang et al., 2004; Shcherbo et al., 2007).

In such applications, RFPs emitting light in the far-red spectral region are preferable, as light with longer wavelengths can penetrate tissue without major attenuation due to absorption and scattering. Moreover, their emission wavelengths are well separated from cellular autofluorescence (Billinton and Knight, 2001) and the fluorescence of many pharmaceutically relevant compounds. Several far-red-emitting FPs have been reported thus far. A far-red-emitting variant of DsRed, designated mPlum, with excitation and emission maxima at 590 nm and 649 nm, respectively, was developed by in vivo mutagenesis by using somatic hypermutation (Wang et al., 2004). A number of essentially nonfluorescent chromoproteins from sea anemones were converted to far-red FPs by introduction of serine at position 143 (corresponding to H148 in GFP) (Gurskaya et al., 2001). This mutational strategy also yielded the mutant AQ14 of the blue chromoprotein aeCP597 from *Actinia equina*, which had the most red-shifted emission maximum, at 663 nm, of all RFPs available to date (Shkrob et al., 2006). Although chemical instability makes the protein unsuitable for cell biological applications, it demonstrates how far the emission of a DsRed-like chromophore can be red shifted without further extension of the conjugated π-electron system.

We previously introduced the far-red-emitting FP eqFP611 from the sea anemone *Entacmaea quadricolor*, which has a number of interesting properties such as the most red-shifted emission of all RFPs from natural sources hitherto identified, a large Stokes shift (52 nm), low aggregation tendency, and virtually complete absence of the green-emitting species (Wiedenmann et al., 2002). However, eqFP611 only folds properly at temperatures below 30°C (Wiedenmann et al., 2002, 2005) and is, therefore, of limited use in experiments involving mammalian cultured cells. Overall, eqFP611 appears to be a promising lead structure for the development of advanced marker proteins. A closely related protein from *E. quadricolor*, eqFP578, was recently converted into a bright, far-red-emitting variant named Katushka (Shcherbo et al., 2007). In view of the wide applicability of far-red-emitting FPs, further development and optimization is advised (Table 1), for example, to create markers with bright emission around 660 nm and beyond. Detailed investigations of far-red-emitting FP variants are required to develop strategies to further advance these fluorescent markers. By using a mutational analysis of eqFP611 that combines directed and random approaches, we have succeeded in generating brightly fluorescent and highly stable variants folding at 37°C, with their fluorescence emission maxima shifted up to 639 nm. The mutant proteins were subjected to a detailed spectroscopic study and tested in cell biological applications.

RESULTS AND DISCUSSION

Mutational Analysis

Although eqFP611 is brightly fluorescent, it is most similar to actiniarian nonfluorescent chromoproteins with regard to its primary sequence; it shares 59.3% identical residues with its closest homolog, asCP562 (Wiedenmann et al., 2000). The phenolate side chain of the chromophore-forming tyrosine of eqFP611 adopts a *trans* conformation, as was observed for several chromoproteins (Prescott et al., 2003; Quillin et al., 2005; Andresen et al., 2005). This conformation is stabilized by hydrogen bonds

of the phenolate oxygen to N143 and S158. The bright fluorescence has been attributed to the planarity of the chromophore (Petersen et al., 2003; Nienhaus et al., 2003). Considering the structural similarity of eqFP611 with actiniarian chromoproteins and its ability to convert to the *cis* state upon irradiation (Loos et al., 2006), we anticipated that the N143S substitution should induce a *trans-cis* isomerization, accompanied by a red shift of the fluorescence. Indeed, this mutant was found to show strong red fluorescence with excitation and emission peaks at 583 and 630 nm, respectively (Figure 1A; Table 1). Random mutagenesis of the homologous position in eqFP578 revealed that serine is most effective in inducing the red shift of the fluorescence (Shcherbo et al., 2007). The N143S mutant of eqFP611 was denoted as RFP630, in which the acronym RFP stands for "red fluorescent protein" and the associated number indicates the peak emission wavelength. This nomenclature was extended to all eqFP611 mutants generated in the present study. X-ray structure analysis was performed on RFP630 crystals; the electron density map at 2.1 Å resolution clearly reveals that the phenolate group of the chromophore is predominantly in the *cis* conformation (K.N. et al., unpublished data).

Although eqFP611 was successfully employed as a marker protein, for instance in yeast and tobacco (Schiebel and Maekawa, 2004; Janke et al., 2004; Forner and Binder, 2007), its restricted expression temperature to below 30°C complicates its application as an in vivo marker in mammalian expression systems. The lack of folding at 37°C was also observed for the redshifted variant, RFP630. To extend the temperature range, we subjected both eqFP611 and RFP630 to random mutagenesis. Approximately 360,000 bacterial colonies were screened for red fluorescence after overnight growth on agar plates at 37°C. Out of 41 improved variants, 2 mutant proteins showed especially bright fluorescence, 1 eqFP611 variant and 1 variant of RFP630.

The fluorescence of the folding-optimized eqFP611 variant is characterized by excitation and emission maxima at 559 and 611 nm, respectively (Figure 1B; Table 1). Consequently, this variant was named RFP611. DNA sequencing revealed that the protein carries two mutations, I57V and F102I. The side chains of both amino acids form the interior of the β can. The folding is mainly promoted by the substitution F102I, demonstrated by the fact that the single mutant readily folds at 37°C. Saturation mutagenesis of position 102 showed that substitutions by leucine or valine also improve the fluorescence at 37°C, though less markedly. It is noteworthy that all beneficial substitutions contain smaller aliphatic side chains. DsRed and Katushka, both capable of folding at 37°C, carry valine or leucine at the homologous positions (Matz et al., 1999; Shcherbo et al., 2007). Moreover, Yanushevich et al. (2002) described the corresponding V105A mutation as the one accelerating the maturation of DsRed. Therefore, this residue appears to play a key role in engineering RFPs.

The mutant of RFP630 folding best at 37°C was found to contain the amino acid exchanges S171F and V184D. However, the emission spectrum of this variant is again shifted back to blue; it has a peak around 618 nm. Consequently, this variant was named RFP618. Its excitation spectrum shows maxima at ∼560 and ∼582 nm, which suggests the presence of a mixture of *cis* and *trans* isomers of the chromophore (Figure 1C). Interestingly, the fluorescence spectrum was sometimes found to be shifted either

Table 1. Far-Red-Emitting FPs and Their Properties

FP Variant	Excitation Maximum (nm)	Emission Maximum (nm)	QY	E_{mol} (M^{-1} cm^{-1})	Relative Brightness[a]	$t_{0.5}$ Maturation at 37°C (hr)	Photobleaching Probability $\times 10^6$
eqFP611 (Wiedenmann et al., 2002)	559	611	0.45	116,000[b], 146,000[c]	1.64[b], 2.07[c]	n.a.	6.5[d]
RFP611	559	611	0.48	120,000[b], 151,000[c]	1.81[b], 2.3[c]	1.83	4.9
td-RFP611	558	609	0.47	70,000[b], 144,000[c]	1.04[b], 2.13[c]	3.75	3.4
RFP630	583	630	0.35	50,000[b]	0.55	n.a.	n.d.
RFP618	560/582	618	0.35	n.a.	n.a.	<8[e]	n.d.
d-RFP618	560/582	618	0.35	n.a.	n.a.	<8[e]	n.d.
RFP637	587	637	0.23	72,000[b], 141,300[c]	0.52[b], 1.02[c]	<8[e]	n.d.
RFP639	588	639	0.18	69,000[b], 110,400[c]	0.39[b], 0.63[c]	1.5	1.3
td-RFP639	589	631	0.16	90,400[b], 110,000[c]	0.46[b], 0.55[c]	<8[e]	1.6
AQ14 (Shkrob et al., 2006)	595	663	-	-	-	-	-
mPlum (Wang et al., 2004)	590	649	0.1	41,000[b], 143,400[c,f]	0.13[b], 0.45[c,f]	1.66	0.9[f]
hcRed (Gurskaya et al., 2001)	594	645	0.05	70,000[b]	0.11		-
Katushka (Shcherbo et al., 2007)	588	635	0.34	65,000[b]	0.70	0.33	-
mKate (Shcherbo et al., 2007)	588	635	0.33	45,000[b]	0.47	1.25	-
mRaspberry (Wang et al., 2004)	598	625	0.15	86,000[b]	0.41	0.92	-
mCherry (Shaner et al., 2004)	587	615	0.22	72,000[b]	0.5	0.25	4.0[f]

[a] Product of QY and E_{mol} compared to the brightness of EGFP (53,000 M^{-1} cm^{-1} $\times$ 0.60) (Patterson et al., 1997).
[b] Concentration of the red chromophore determined by the alkaline denaturation method (Gross et al., 2000).
[c] Concentration of the red chromophore determined by the dynamic difference method.
[d] The value reported previously by Schenk et al. (2004) is larger by a factor of $\sim$3, which may be due to the high-intensity, focused laser illumination used for bleaching individual molecules.
[e] Determined from expression in HEK293 cells.
[f] Values determined during the present study.

toward 611 or 630 nm, depending on the preparation, indicating that subtle variations of the expression conditions influence the ratio between *cis* and *trans* states. The mutation V184D is located in a flexible loop region (Petersen et al., 2003; Nienhaus et al., 2003). The substitution might promote folding by forming a hydrogen bond with the G152 carbonyl from the neighboring loop structure, resulting in stabilization of the loop. The S171F mutation, which enables expression of RFP618 at 37°C, obviously affects A/C interface interactions, as the hydroxyl group of S171 is located within 4.0 Å of Y157 of the adjacent protomer. The newly introduced phenyl group presumably stabilizes the interface via hydrophobic and π-stacking interactions with Y157. This suggestion is supported by the observation that A/C interactions are especially beneficial to folding of eqFP611 (Wiedenmann et al., 2005). Strengthening of the A/C interfacial interactions by S171F exchange may further introduce a subtle repositioning of the side chain of the key residue S143, which is also localized in the A/C interface, thereby shifting the equilibrium between *cis* and *trans* conformations of the chromophore. Moreover, the fraction of molecules with green fluorescence increased significantly, indicating that maturation of the red chromophore is adversely affected by this modification (Figure 1C). As the phenolate side chain of the chromophore is stabilized in the *trans* conformation by hydrogen bonding to N143 and S158 in wild-type eqFP611, we subjected residue Ser158 of RFP618 to random mutagenesis to disrupt the hydrogen bond, which should shift the equilibrium toward the far-red-emitting *cis* conformation of the chromophore. Analysis of the mutant library revealed that

two substitutions, alanine and cysteine, were most efficient in shifting the emission maxima to 637 (S158A) and 639 nm (S158C), respectively. Therefore, these mutants were named RFP637 and RFP639. Their excitation spectra show single bands at 587 nm (RFP637) (Table 1) and 588 nm (RFP639) (Figure 1D; Table 1), indicating that the phenolate group of Tyr64 predominantly adopts the *cis* conformation. Moreover, the amount of the green fluorescent form is significantly reduced, indicating that maturation of the red chromophore is improved (Figure 1D). Apparently, the removal of the hydrogen bond due to the S158A mutation shifts the chromophore completely to the *cis* conformation. Despite its structural similarity to serine, the cysteine substitution has the same effect due to the reduced hydrogen-bonding capability of the thiol group. The combination Ala/Cys158 with Ser143 was earlier reported to red shift the fluorescence of aeCP597 (Shkrob et al., 2006). As the spectral properties of RFP637 and RFP639 are very similar, we have restricted ourselves only to RFP639 for an in-depth characterization of its spectroscopic properties. The mutations and their effects on folding and emission wavelength are summarized for all eqFP611 variants in Table 2.

Characterization of the Mutant FPs' Response to Low pH
The red fluorescence of the eqFP611 derivatives remains essentially unaffected by lowering the pH from 8.0 to 5.0, as was already observed for the wild-type protein (Figure 2) (Wiedenmann et al., 2002). Below pH 4, RFP611 shows an absorption increase at $\sim$370 nm at the expense of the 557 nm band (Figure 2A). In
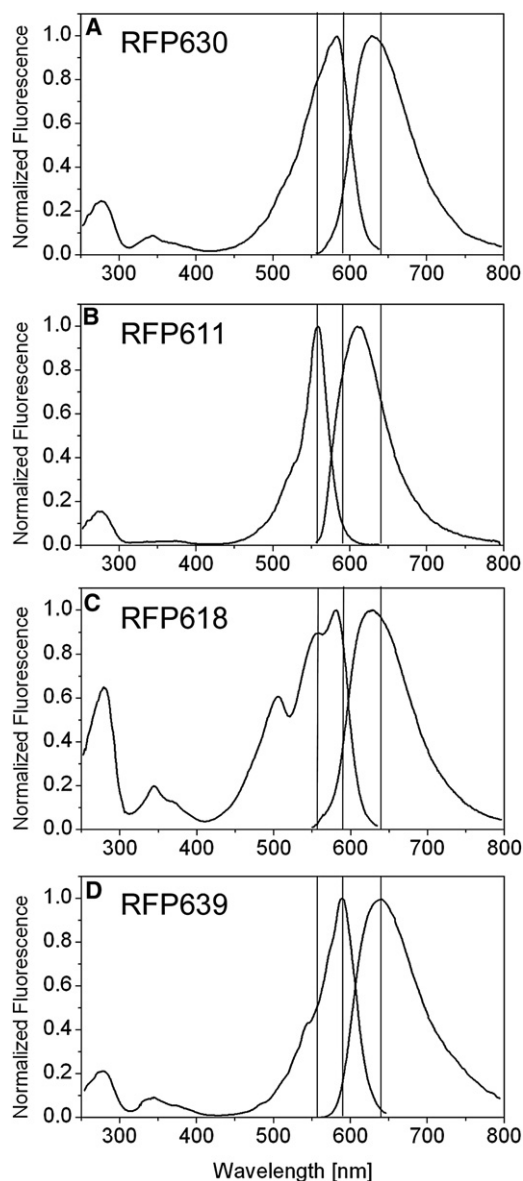
Figure 1. Fluorescence Properties of eqFP611 Derivatives
(A–D) Excitation and emission spectra of (A) the red-shifted mutant RFP630, (B) the folding-optimized variant RFP611, (C) the folding-optimized variant RFP618, and (D) the folding-optimized, red-shifted variant RFP639. Vertical lines mark the positions of the excitation peaks of eqFP611 (559 nm) and RFP639 (588 nm) and the emission peak of RFP639 (639 nm).

Table 2. Mutations and Their Effects in eqFP611 Variants

eqFP611 Variant	Optimization of Folding	Red Shift of Fluorescence	Dimerization
RFP611	I57V, F102I	-	-
RFP630	-	N143S	-
RFP618	S171F, V184D	N143S	-
RFP637	S171F, V184D	S158A, N143S	-
RFP639	S171F, V184D	S158C, N143S	-
td-RFP611	I57V, F102I, S171F, V184D	-	T122R
d-RFP618	S171F, V184D	N143S	T122R
td-RFP639	S171F, V184D	S158C, N143S	T122R

increase of the absorption at ~390 nm associated with the decrease of the 513 nm band (Figure 2C). This two-state process results in a crisp isosbestic point at 450 nm. At pH < 5, the 583 nm band decreases due to the appearance of a protonated red chromophore, which is associated with a minor band at 450 nm. Most protonated red chromophores, however, decompose; their acylimine bonds are reduced to form the protonated 4-(p-hydroxybenzylidene)-5-imidazolinone core of the chromophore, resulting in a further increase of the band at 390 nm. The spectral changes in Figure 2C involve more than two states, and, therefore, an isosbestic point is not visible for the complete range of pH values. From the spectra, it is also evident that the protonation reactions of the green and red chromophores have markedly different pK values.

The absorption spectrum of RFP639 shows only a weak shoulder at 513 nm and hence a smaller fraction of green chromophores than RFP630 (Figure 2E); they protonate between pH 8 and 6, as in RFP630. In contrast to RFP630, however, is the finding that the decrease at 588 nm below pH 4 is accompanied by a pronounced increase of the band of the protonated red chromophore at ~450 nm. Incubation at pH ~2 for more than 5 min finally reduces all acylimine bonds and yields only protonated GFP chromophores. Again, isosbestic points are absent, indicative of the involvement of more than two chromophore states. Comparison with RFP611 suggests that the *cis* conformation of the red chromophore in RFP639 helps stabilize the protein scaffold at low pH, thereby protecting the acylimine bond from immediate reduction or hydrolysis. A stabilizing effect of the *cis* conformation is further evident from the considerable absorption of the red chromophore at pH 3 (Figure 2F), at which the red chromophore of RFP611 is already hydrolyzed (Figure 2B). The eqFP611 mutants are considerably more stable at low pH than the red-shifted derivatives of eqFP578 (Shcherbo et al., 2007); both Katushka and mKate are essentially nonfluorescent at pH 5.

Characterization of the Mutant FPs' Response to High pH

The alkaline denaturation transition can be observed in the absorption spectrum of RFP611 at pH 11.5 (Figure 3A). In an initial 30 min period, the small amount of the green form denatures along with a fraction of the red chromophore, as inferred from the increase of the typical ~450 nm absorption band of the alkaline-denatured GFP chromophore at the expense of the absorption bands at ~500 and 557 nm. Therefore, an isosbestic point is

combination with the absence of an ~450 nm band indicative of the protonated red chromophore, this observation suggests that the acylimine bond becomes hydrolyzed or at least reduced at low pH. A breakdown of the acylimine bond was also reported for DsRed and the chromoprotein RTMS5 at the high and low pH extremes (Gross et al., 2000; Turcic et al., 2006).

The behavior of RFP630 toward low pH appears to be rather complex (Figure 2C). A pronounced shoulder at ~513 nm in the absorption spectrum indicates the presence of a green fluorescent species. From pH 8 to 6, exclusively the green chromophore converts to its protonated form, as can be inferred from the

Figure 2. Response of the Absorption of eqFP611 Derivatives to low pH Conditions
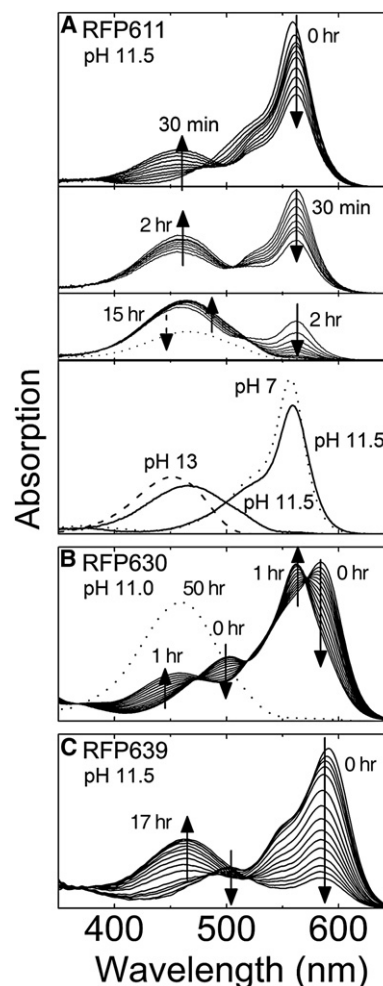
(A–F) (A and B) RFP611, (C and D) RFP630, and (E and F) RFP639. The left column shows the absorption spectra at various pH values. Spectra were recorded immediately after adjusting the protein to a certain pH value. In (C), the absorption of RFP639 at pH 2.1 was recorded immediately (pH 2.1A) and after 5 min (pH 2.1B). The absorption of the red chromophores shown in the right column was normalized to equal peak values.

Figure 3. Response of eqFP611 Derivatives to High pH Conditions

(A) The time-dependent changes in the absorption spectrum of RFP611 at pH 11.5 can be divided into three phases. Uppermost panel: Phase 1, decrease of the absorption at ~500 and ~559 nm and increase of the absorption at ~450 nm; 2nd panel: Phase 2, decrease of the absorption at ~559 nm and increase of the absorption at ~450 nm; 3rd panel: Phase 3, decrease of the absorption at ~559 and ~450 nm. Panel 4: the amplitude and wavelength of the absorption maximum of the native and alkaline-denatured chromophore of RFP611 are pH dependent.

(B) The maximum absorbance of the red chromophore of RFP630 changes from ~583 nm to ~559 nm within the first hour of incubation at pH 11.0.

(C) Time course of the alkaline denaturation of RFP639 at pH 11.5.

absent. In a second phase, from 0.5 to 15 hr, only the remaining red fluorescent chromophore is converted to the GFP chromophore, as can be inferred from the crisp isosbestic point at ~502 nm. After ~15 hr, the decrease of the absorption at ~450 nm reflects significant degradation of the GFP chromophore.

A completely different response to high pH is observed for RFP630 (Figure 3B). During incubation at pH 11.5 for 1 hr, the 583 nm band decreases, and, concomitantly, a peak appears at ~559 nm, the absorption maximum of the *trans* chromophore of eqFP611. This observation indicates a pH-dependent *cis-trans* isomerization. Commonly, isomerization of the chromophore was found to be driven by light in eqFP611, KFP, and Dronpa (Andresen et al., 2005; Loos et al., 2006; Andresen et al., 2007). Along with the isomerization of the red chromophore, the green form already denatures, as inferred from the increase of the ~450 nm absorption band at the expense of the band at ~500 nm. After 50 hr, the absorption spectrum consists of a single broad band at ~450 nm, indicating that the protein completely denatured and the acylimine bond of the chromophore is reduced.

RFP639 displays yet another spectral response to high pH (Figure 3C). Compared to RFP630, the S158C mutation led to a strong reduction of the absorption at ~500 nm. The alkaline denaturation of the remaining green fluorescent species occurs within 20 min of incubation at pH 11.5, masking the isosbestic point that should normally appear upon breakdown of the red chromophore. After this phase, the ~450 nm band continuously

increases at the expense of the absorption at 588 nm. Remarkably, the 559 nm absorption band of wild-type eqFP611 never appeared during the course of denaturation. This spectral response is clearly different from that of RFP630 and underscores the success of the S158C substitution in stabilizing the *cis* conformation of the chromophore.

Determination of Molar Extinction Coefficients

Methods for determining the molar extinction coefficient of FPs rely on protein quantification based on the absorption at 280 nm or on biochemical determination methods such as the Nano-Orange assay (Matz et al., 1999; Wiedenmann et al., 2002;

Ward, 2005). As these methods also include misfolded proteins or those with immature chromophores, the concentration of proteins with functional chromophores is usually overestimated, and, consequently, the extinction coefficients are artificially decreased. Currently, the method considered most accurate for determining the extinction coefficients of GFP-like proteins measures the absorption of the chromophore at 447 nm in 0.1 N NaOH (Gross et al., 2000; Ward, 2005) to 2 N NaOH (Shcherbo et al., 2007) and uses the extinction coefficient of denatured GFP at pH 13 to calculate the protein concentration (Ward, 2005). Hence, this value includes only mature proteins with a functional chromophore. This alkaline denaturation method works accurately only if a single chromophore species is converted completely to the alkaline-denatured form absorbing at ~447 nm. Moreover, the GFP-like chromophore must be stable in 0.1–2.0 N NaOH solutions. Our measurements of eqFP611 variants reveal that the alkaline denaturation of both green and red fluorophores gives rise to the ~450 nm absorption band (Figures 3A–3C). Consequently, if green fluorescent and possibly nonfluorescent species are present in an RFP sample, the concentration of the functional red chromophore will again be overestimated, and the derived molar extinction coefficient will come out too low.

Ward (1981) already reported degradation of the GFP chromophore at pH 13 within 30–60 min. For several variants of eqFP611, we also observed an absorption decay at ~450 nm in 0.1 N NaOH on a timescale of minutes, reflecting degradation of the green chromophore. Also, denaturation in 1 N NaOH strongly decreased the absorption at ~450 nm. In these cases, the concentration of the functional red chromophore will be assumed to be too low, and the extinction coefficients will be inaccurately high. In order to eliminate these experimental errors, we have developed a dynamic difference method based on the recording of time-dependent denaturation at moderately alkaline pH.

In a first step, we determine the pH at which time-resolved measurements of the alkaline denaturation can be performed in the spectrophotometer without degrading the denatured GFP chromophore (Figure 3). This value ranges between pH 11 and 13, depending on the stability of the particular FP. The first phase of the denaturation involves the decay of both green and red chromophores. As soon as a crisp isosbestic point appears, we can be sure that all spectral changes result from the denaturation of only the red chomophore. We calculate the decrease in the major absorption band of the red chromophore for several time intervals and relate each to the corresponding increase of the absorption at ~450 nm to obtain the ratio of the extinction coefficients at ~450 nm and the native absorption band. Subsequently, the protein solution is adjusted to pH 13 to determine the ratio between the extinction coefficients at the actual sample pH and pH 13. The maximal extinction coefficient at pH 13 was set to the literature value of 44,000 $M^{-1} \cdot cm^{-1}$ (Ward, 2005). This ratio was then used to calculate the concentration of chromophore molecules and to determine the extinction coefficient of the native absorption band at the sample pH. In a final step, a new sample with identical protein concentration was prepared to rescale the extinction coefficients of the native absorption band at the actual pH of the sample to the one at pH 7.

By using the dynamic difference method, we obtained an extinction coefficient of the red chromophore of mPlum of 143,400 $M^{-1} \cdot cm^{-1}$, which is drastically larger than other published values ranging from 22,000 to 41,000 $M^{-1} \cdot cm^{-1}$ (Shcherbo et al., 2007). The discrepancy follows directly from the high content of green fluorescent chromophores in mPlum preparations. (Figure S1; see the Supplemental Data available with this article online). Interestingly, the high amount of green fluorescent species was only observed for mPlum expressed in bacteria, but not in HEK293 cells, at 37°C. It is interesting to note that Gross et al. (2000) have earlier reported a similar E_{mol} of 150,000 $M^{-1} \cdot cm^{-1}$ for the red chromophore of DsRed. In their approach, the amount of green fluorescent species was deduced from mass spectroscopic analysis of the chromophore-containing peptides obtained by protease treatment of DsRed and from the amount of protein resistant to cleavage by boiling at extreme pH (indicative of the absence of the acylimine bond). Subsequently, the "contaminating" protein species were subtracted from the total protein concentration to obtain only the concentration of the RFP.

Brightness, Maturation Time, and Photostability

Using the dynamic difference method, we determined extinction coefficients of 151,400 $M^{-1} \cdot cm^{-1}$ for RFP611, 141,300 $M^{-1} \cdot cm^{-1}$ for RFP637, and 110,400 $M^{-1} \cdot cm^{-1}$ for RFP639 (Table 1). With a quantum yield of 0.48, RFP611 shows an excellent brightness. The quantum yields of RFP637 (0.23) and RFP639 (0.18) are higher than those of other far-red FPs, such as mPlum, hcRed, and AQ143 (Table 1). In combination with the high extinction coefficients, the red-shifted eqFP611 derivatives are among the brightest far-red-emitting FPs currently available (Table 1; Shcherbo et al., 2007).

We have also measured the time required for folding and maturation of the chromophores of recombinantly expressed RFP611 and RFP639 at 37°C (Table 1). With a half-life of ~2 hr, the maturation times are somewhat slower than those reported for other engineered anthozoan RFPs (Shaner et al., 2004; Merzlyak et al., 2007; Shcherbo et al., 2007), but faster than DsRed2 (6.5 hr) (Clontech, 2001) and mOrange (2.5 hr) (Shaner et al., 2004).

Finally, we tested the photostability of RFP611 and RFP639 by exciting purified protein samples with a defocused 532 nm Nd-YAG laser beam and measuring the decay of the red fluorescence. Data were subsequently corrected for the absorption of the chromophores at 532 nm. The bleaching rate of RFP611 is similar to mCherry (Table 1) and lower than that of wild-type eqFP611. Interestingly, RFP639 is characterized by a very low bleaching rate. The resistance against photobleaching might be due to the increased stability of the molecule inferable from the stability at pH extremes. A relation to the particular conformation of the chromophore might exist, as the red-shifted variants of eqFP578 (mKate) (Shcherbo et al., 2007) and DsRed (mPlum) are also characterized by a comparably high photostability (Table 1).

Dimeric Variants

Although tetrameric FPs have been successfully applied as fusion markers (Wiedenmann et al., 2004; Schiebel and Maekawa, 2004), there is always a concern that oligomerization interferes with the function of the fusion partner. Dimeric variants of eqFP611 with essentially identical spectral properties were produced by introducing the A/B interface mutations T122R and
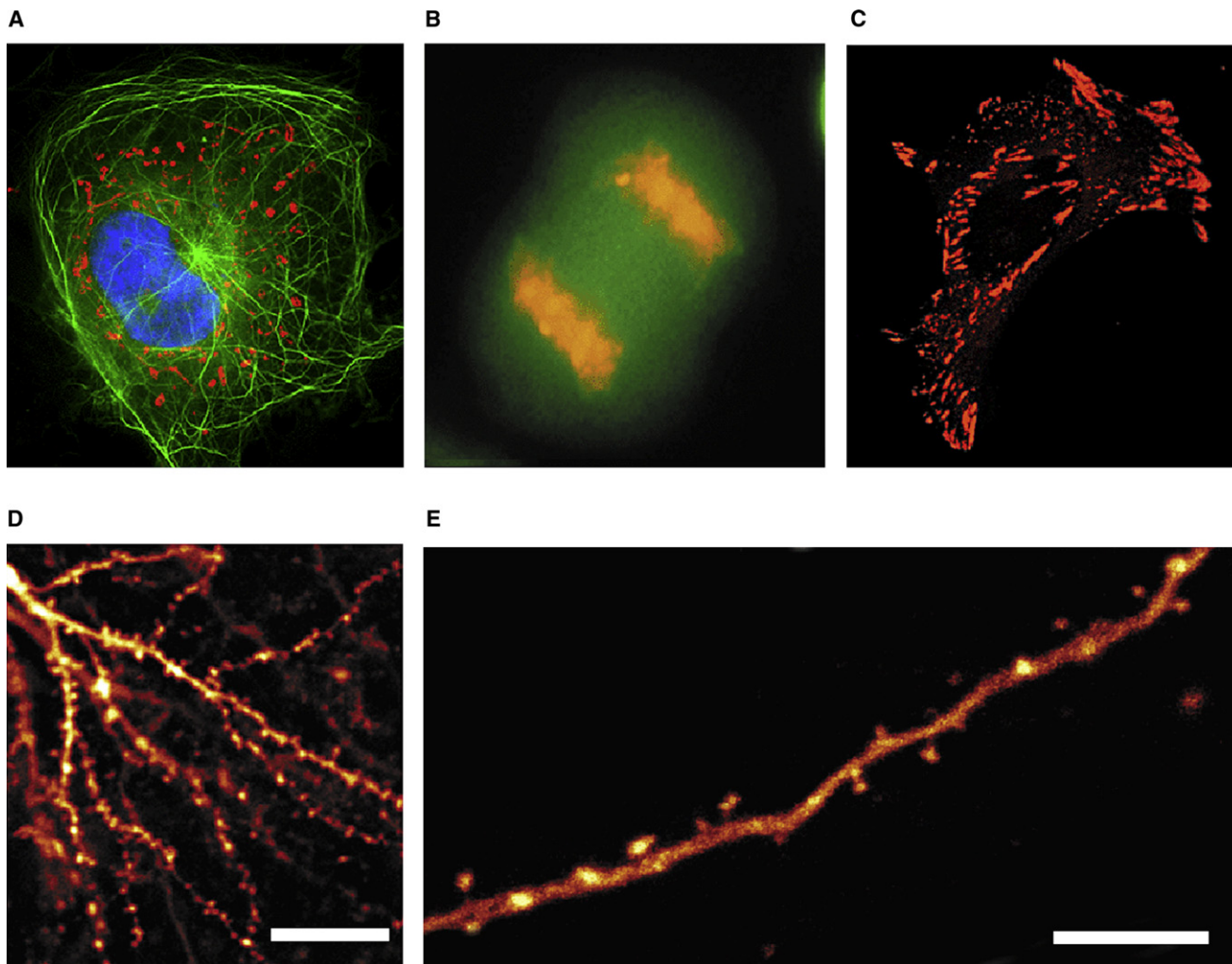
Figure 4. Applications of eqFP611 Variants as Cellular Labels

(A) Three-color imaging with RFP611, EGFP, and DAPI in HeLa cells. Mitochondria are highlighted in red by RFP611 fused to a mitochondrial localization signal. Tubulin fibers are marked green by an EGFP-labeled tubulin-associated protein. The nucleus was stained blue with DAPI.

(B) Chromatin association of RBP-2N-RFP611 in mitotic HEK293 cells. EGFP is localized in the cytoplasm.

(C) Localization of the paxillin-RFP611 fusion in focal adhesion spots of HEK293 cells.

(D) Two-photon excitation (1030 nm) of dimeric RFP618 expressed in dendrites of murine pyramidal cells upon infection with a modified Sindbis virus (false color image, the scale bar is 10 μm).

(E) Magnified view of a single dendrite with dendritic spines (the scale bar is 6 μm).

V124T (Wiedenmann et al., 2005). As none of the mutations promoting proper folding appear to function by enforcing A/B interactions, we anticipated that this strategy would also yield dimeric variants of RFP611 and RFP637 that can be functionally expressed at 37°C. Indeed, the substitution T122R produced variants that eluted with the apparent molecular mass typical of dimeric FPs from a gel-filtration column (Wiedenmann et al., 2005). It was also possible to construct pseudo monomeric tags by fusing dimeric variants via a 12 amino acid linker (Campbell et al., 2002; Fradkov et al., 2002). The brightness and maturation speed of the bacterially expressed dimers (d-RFPs) and tandem dimers (td-RFPs) is only slightly affected by the process of dimerization (Table 1). These results encourage further engineering to obtain truly monomeric variants of eqFP611.

Applications of eqFP611 Variants as Cellular Markers

We further tested the new RFPs for their performance in cellular imaging applications. When fused to the mitochondrial targeting sequence from subunit VIII of cytochrome c oxidase, the tetrameric RFP611 displayed bright red fluorescence without affecting cellular viability. Three-color imaging in combination with EGFP and DAPI could be readily achieved (Figure 4A). Despite the tetrameric nature of the tag, fusion with RBP-2N shows the typical strong binding to chromatin (Figure 4B) (Wiedenmann et al., 2004), highlighting the chromosomes during mitosis. The identical distribution was observed for RBP-2N fusions with EGFP. Also, fusions with paxillin localized correctly in focal adhesion spots (Figure 4C) (von Wichert et al., 2003). The fact that even the tetrameric protein can be used as a fusion marker

indicates the absence of any aggregation tendency. The dimeric tags can also be successfully applied as markers for labeling of cells in two-photon imaging applications, as demonstrated for d-RFP618: expressed in rodent organotypic slice cultures, the engineered FP allowed for high-resolution imaging of the spines of dendritic branches of hippocampal pyramidal cells with 1030 nm light for two-photon excitation (Figures 4D and 4E). The successful application as tissue marker in *Xenopus laevis* (Shcherbo et al., 2007) and the good performance in two-photon imaging demonstrated here further stress the potential of *Entacmaea*-derived far-red FPs for the development of advanced whole-body imaging markers. To this end, far-red eqFPs are ideal candidates for in vivo mutagenesis.

SIGNIFICANCE

Fluorescent proteins homologous to the green fluorescent protein (GFP) are widely employed in biomedical research as in vivo markers. Additionally, they are excellent model systems by which to explore basic photophysical and photochemical mechanisms mediating chromophore formation and protein fluorescence. Emission colors of natural GFP variants and their mutants generated by biotechnological engineering cover a broad spectral range from blue to red. However, marker proteins with even further red-shifted emission are desirable, especially for tissue and whole-body imaging. Their development requires an understanding of the biophysical prerequisites of far-red fluorescence.

We have mutated the red fluorescent protein eqFP611 and obtained folding-optimized and red-shifted variants. The red shift is caused by a *trans-cis* isomerization of the phenolate group of the chromophore. Most interesting, the present case gives a rare example of GFP-like proteins in which both *cis* and *trans* isomers are brightly fluorescent. An approach was introduced that allows for a more accurate determination of the molar extinction coefficients of red fluorescent GFP-like proteins. The high extinction coefficients and quantum yields of the red-shifted variants place these eqFP611 derivatives among the brightest far-red FPs currently available. Cellular applications revealed neither signs of aggregation nor adverse effects on cellular viability. Their brightness and stability at pH extremes and under intense irradiation makes these proteins promising lead structures for the development of even further red-shifted FPs.

EXPERIMENTAL PROCEDURES

Mutagenesis and Vector Construction
Random mutagenesis was carried out according to the manufacturer's protocol by using the Diversify PCR Random Mutagenesis Kit (BD Bioscience Clontech, Palo Alto, CA, USA) in conditions optimal for 4–5 mutations per 1000 bp. The coding sequences of eqFP611 and RFP630 inserted in the pQE32 expression vector (QIAGEN, Hilden, Germany) were used as templates. Site-directed mutagenesis of the eqFP611 template was performed by overlap extension PCR (Ho et al., 1989) by using sense and antisense oligonucleotides carrying the desired mutation(s) in combination with primers flanking the open reading frame. Tandem constructs of the eqFP611 mutant were generated by connecting two copies of cDNA of a folding-optimized, dimeric (T122R) variant by a linker sequence coding for the amino acids GHGTGSTGSGSS (Campbell et al., 2002). For eukaryotic expression, the cDNA coding for the marker or fusion proteins was cloned in the pcDNA3 vector (Invitrogen, Carlsbad, CA,

USA). Bacterial expression was set up with the pQE32 vector (QIAGEN, Hilden, Germany).

Fluorescence of bacterial colonies expressing eqFP611 variants was monitored with a UVA transilluminator (365 nm) and a fluorescence microscope (Axioplan I, Carl Zeiss Jena GmbH, Jena, Germany).

Protein Expression and Purification
All proteins were expressed in *E. coli* (M15 pREP4 or BL21 DE3) as described (Wiedenmann et al., 2002, 2005) and were purified by using a Talon metal-affinity resin (BD Biosciences Clontech, Palo Alto, CA, USA) and gel filtration (Superdex 200, Äkta-System, Amersham Pharmacia, Little Chalfont, United Kingdom). Prior to determination of the apparent molecular weights of the fluorescent proteins, the column was calibrated with carbonic anhydrase, bovine serum albumin, alcohol dehydrogenase, blue dextran (Sigma-Aldrich, Steinheim, Germany), avGFP, and DsRed as standards.

Spectroscopy
The initial spectral characterization was performed in PBS buffer (pH 7.5). For the pH-dependent studies, a few microliters of a concentrated protein stock solution were added to 100 mM buffer of the desired pH (pH < 4.5, sodium phosphate/citrate; pH 5–8.5, sodium phosphate; pH > 8.5, sodium carbonate) to obtain a final protein concentration of ~10 μM. Data collection was initiated immediately after mixing. Especially at the extreme pH values, each spectrum was recorded repeatedly to account for possible spectral changes on timescales similar to the experimental timescale (~1 min).

Absorption spectra were recorded on a Cary 1 spectrophotometer (Varian, Darmstadt, Germany) with a resolution of 1 nm. Fluorescence excitation and emission spectra were measured on a SPEX Fluorolog II spectrofluorometer (Spex Industries, Edison, NJ, USA) with the excitation line width set to 0.85 nm. Emission spectra were recorded with 2.2 nm resolution and corrected for the wavelength dependence of the detector efficiency.

Determination of Maturation Times
E. coli M15 pREP4 were grown in 2YT medium at 37°C. Expression of the proteins was induced by adding IPTG to a final concentration of 0.5 mM as soon as the culture reached an optical density of $OD_{600} = 0.7$. The cells were harvested after 1 hr, and the proteins were quickly purified by metal-affinity chromatography as described earlier (Wiedenmann et al., 2002). Purification was performed at 4°C, and all solutions were kept on ice. Subsequently, the purified protein solutions were incubated at 37°C, and the maturation time course was recorded in a Cary Eclipse Spectrofluorometer (Varian, Darmstadt, Germany).

Determination of Extinction Coefficients and Quantum Yields
The detailed protocol for the determination of extinction coefficients is given in the Results and Discussion. The quantum yields were determined as described previously (Wiedenmann et al., 2002).

Photobleaching
For the photobleaching experiments, 20 μl dilute protein solution (concentration ~1 μM) was filled into a 1 × 10 × 30 mm quartz cuvette and illuminated with 532 nm light from a SuwTech LDC-2500 laser emitting 70 mW. The laser was carefully adjusted to illuminate the entire sample volume. The fluorescence intensity was recorded at 610 nm (640 nm for RFP639 and td-RFP639) as a function of time by using a SPEX Fluorolog II spectrofluorometer (Spex Industries, Edison, NJ, USA). The bleaching kinetics were fitted with a stretched exponential,

$$y = A_1 \cdot \exp(-(\tau/t)^\beta) + A_0. \tag{1}$$

Average bleaching times, $<\tau>$, were determined according to

$$<\tau> = \frac{\tau}{\beta}\Gamma\left(\frac{1}{\beta}\right), \tag{2}$$

where Γ indicates the gamma function. From these values, the photobleaching probabilities, Φ, were calculated, taking $\Phi(R6G) = 2.5 \times 10^{-6}$ as a reference (Eggeling et al., 2005).

Eukaryotic Expression and Imaging

Cell lines were grown on chambered cover glasses (Nalge Nunc International Corp., Rochester, NY, USA) and transfected with 500 ng vector DNA. HEK293 cells were transfected with the calcium phosphate coprecipitation technique; HeLa cells were transfected with the FuGENE transfection reagent (Roche Diagnostics, Mannheim, Germany). Cells were grown at 37°C under 5% CO_2 in Dulbecco's modified Eagle's medium (Invitrogen, Carlsbad, CA, USA) supplemented with 10% fetal calf serum. Cells were imaged 24 hr after transfection by using a fluorescence microscope (DM IRB, Leica Microsystems, Wetzlar, Germany) equipped with a digital camera (C4742, Hamamatsu, Hamamatsu, Japan) and a 100-W mercury lamp. Green and red fluorescence was imaged by using standard FITC and TRITC filter sets.

Sindbis Generation, Infection, and Two-Photon Imaging

The cDNA of the dimeric RFP618 was subcloned in a modified pSinRep5 vector. Viral particles expressing the FP were generated as described previously (Jeromin et al., 2003). Organotypic slice cultures from either rat (Sprague Dawley) or mice were prepared at postnatal day 7 and infected after 5–7 days in vitro. Infected slices were imaged 2–3 days after infection on a Leica SP2 equipped with a T pulse laser (Amplitude Systems, Bordeaux, France) with excitation at 1030 nm for two-photon imaging.

SUPPLEMENTAL DATA

Supplemental Data include one figure that is available with this article at http://www.chembiol.com/cgi/content/full/15/3/224/DC1/.

REFERENCES

Andresen, M., Wahl, M.C., Stiel, A.C., Gräter, F., Schäfer, L.V., Trowitzsch, S., Weber, G., Eggeling, C., Grubmüller, H., Hell, S.W., and Jakobs, S. (2005). Structure and mechanism of the reversible photoswitch of a fluorescent protein. Proc. Natl. Acad. Sci. USA *102*, 13070–13074.

Andresen, M., Stiel, A.C., Trowitzsch, S., Weber, G., Eggeling, C., Wahl, M.C., Hell, S.W., and Jakobs, S. (2007). Structural basis for reversible photoswitching in Dronpa. Proc. Natl. Acad. Sci. USA *104*, 13005–13009.

Billinton, N., and Knight, A.W. (2001). Seeing the wood through the trees: a review of techniques for distinguishing green fluorescent protein from endogenous autofluorescence. Anal. Biochem. *291*, 175–197.

Campbell, R.E., Tour, O., Palmer, A.E., Steinbach, P.A., Baird, G.S., Zacharias, D.A., and Tsien, R.Y. (2002). A monomeric red fluorescent protein. Proc. Natl. Acad. Sci. USA *99*, 7877–7882.

Chalfie, M., Tu, Y., Euskirchen, G., Ward, W.W., and Prasher, D.C. (1994). Green fluorescent proteins as a marker for gene expression. Science *263*, 802–805.

Eggeling, C., Volkmer, A., and Seidel, C.A. (2005). Molecular photobleaching kinetics of Rhodamine 6G by one- and two-photon induced confocal fluorescence microscopy. ChemPhysChem *6*, 791–804.

Forner, J., and Binder, S. (2007). The red fluorescent protein eqFP611: application in subcellular localization studies in higher plants. BMC Plant Biol. *7*, 28.

Fradkov, A.F., Chen, Y., Ding, L., Barsova, E.V., Matz, M.V., and Lukyanov, S.A. (2000). Novel fluorescent protein from Discosoma coral and its mutants possesses a unique far-red fluorescence. FEBS Lett. *479*, 127–130.

Fradkov, A.F., Verkhusha, V.V., Staroverov, D.B., Bulina, M.E., Yanushevich, Y.G., Martynov, V.I., Lukyanov, S., and Lukyanov, K.A. (2002). Far-red fluorescent tag for protein labelling. Biochem. J. *368*, 17–21.

Gross, L.A., Baird, G.S., Hoffman, R.C., Baldridge, K.K., and Tsien, R.Y. (2000). The structure of the chromophore within DsRed, a red fluorescent protein from coral. Proc. Natl. Acad. Sci. USA *97*, 11990–11995.

Gurskaya, N.G., Fradkov, A.F., Terskikh, A., Matz, M.V., Labas, Y.A., Martynov, V.I., Yanushevich, Y.G., Lukyanov, K.A., and Lukyanov, S.A. (2001). GFP-like chromoproteins as a source of far-red fluorescent proteins. FEBS Lett. *507*, 16–20.

Henderson, J.N., and Remington, S.J. (2005). Crystal structures and mutational analysis of amFP486, a cyan fluorescent protein from *Anemonia majano*. Proc. Natl. Acad. Sci. USA *102*, 12712–12717.

Ho, S.N., Hunt, H.D., Horton, R.M., Pullen, J.K., and Pease, L.R. (1989). Site-directed mutagenesis by overlap extension using the polymerase chain reaction. Gene *77*, 51–59.

Ivanchenko, S., Glaschick, S., Röcker, C., Oswald, F., Wiedenmann, J., and Nienhaus, G.U. (2007). Two-photon excitation and photoconversion of EosFP in dual-color 4Pi confocal microscopy. Biophys. J. *92*, 4451–4457.

Janke, C., Magiera, M.M., Rathfelder, N., Taxis, C., Reber, S., Maekawa, H., Moreno-Borchart, A., Doenges, G., Schwob, E., Schiebel, E., and Knop, M. (2004). A versatile toolbox for PCR-based tagging of yeast genes: new fluorescent proteins, more markers and promoter substitution cassettes. Yeast *21*, 947–962. Published online October 4, 2007. 10.1002/yea.1142.

Jeromin, A., Yuan, L.L., Frick, A., Pfaffinger, P., and Johnston, D. (2003). A modified Sindbis vector for prolonged gene expression in neurons. J. Neurophysiol. *4*, 2741–2745.

Karasawa, S., Araki, T., Yamamoto-Hino, M., and Miyawaki, A. (2003). A green-emitting fluorescent protein from Galaxeidae coral and its monomeric version for use in fluorescent labeling. J. Biol. Chem. *278*, 34167–34171.

Karasawa, S., Araki, T., Nagai, T., Mizuno, H., and Miyawaki, A. (2004). Cyan-emitting and orange-emitting fluorescent proteins as a donor/acceptor pair for fluorescence resonance energy transfer. Biochem. J. *381*, 307–312.

Clontech (2001). Living Colors™ DsRed2. CLONTECHniques *XVI*, 2–3.

Loos, D.C., Habuchi, S., Flors, C., Hotta, J.I., Wiedenmann, J., Nienhaus, G.U., and Hofkens, J. (2006). Photoconversion in the red fluorescent protein from the sea anemone *Entacmaea quadricolor*: is *cis-trans* isomerization involved? J. Am. Chem. Soc. *128*, 6270–6271.

Lukyanov, K.A., Fradkov, A.F., Gurskaya, N.G., Matz, M.V., Labas, Y.A., Savitsky, A.P., Markelov, M.L., Zaraisky, A.G., Zhao, X., Fang, Y., et al. (2000). Natural animal coloration can be determined by a nonfluorescent green fluorescent protein homolog. J. Biol. Chem. *275*, 25879–25882.

Matz, M.V., Fradkov, A.F., Labas, Y.A., Savitsky, A.P., Zaraisky, A.G., Markelov, M.L., and Lukyanov, S.A. (1999). Fluorescent proteins from nonbioluminescent *Anthozoa* species. Nat. Biotechnol. *17*, 969–973.

Merzlyak, E.M., Goedhart, J., Shcherbo, D., Bulina, M.E., Shcheglov, A.S., Fradkov, A.F., Gaintzeva, A., Lukyanov, K.A., Lukyanov, S., Gadella, T.W., and Chudakov, D.M. (2007). Bright monomeric red fluorescent protein with an extended fluorescence lifetime. Nat. Methods *4*, 555–557.

Nienhaus, G.U., Nienhaus, K., Hölzle, A., Ivanchenko, S., Röcker, C., Renzi, F., Oswald, F., Wolff, M., Schmitt, F., Vallone, B., et al. (2006). Photoconvertible fluorescent protein EosFP: biophysical properties and cell biology applications. Photochem. Photobiol. *82*, 351–358.

Nienhaus, K., Vallone, B., Renzi, F., Wiedenmann, J., and Nienhaus, G.U. (2003). Crystallization and preliminary X-ray diffraction analysis of the red fluorescent protein eqFP611. Acta Crystallogr. D Biol. Crystallogr. *59*, 1253–1255.

Nienhaus, K., Nienhaus, G.U., Wiedenmann, J., and Nar, H. (2005). Structural basis for photo-induced protein cleavage and green-to-red conversion of fluorescent protein EosFP. Proc. Natl. Acad. Sci. USA *102*, 9156–9159.

Nienhaus, K., Renzi, F., Vallone, B., Wiedenmann, J., and Nienhaus, G.U. (2006a). Chromophore-protein interactions in the anthozoan green fluorescent protein asFP499. Biophys. J. *91*, 4210–4220.

Nienhaus, K., Renzi, F., Vallone, B., Wiedenmann, J., and Nienhaus, G.U. (2006b). Exploring chromophore-protein interactions in fluorescent protein cmFP512 from *Cerianthus membranaceus*: X-ray structure analysis and optical spectroscopy. Biochemistry *45*, 12942–12953.

Patterson, G.H., Knobel, S.M., Sharif, W.D., Kain, S.R., and Piston, D.W. (1997). Use of the green fluorescent protein and its mutants in quantitative fluorescence microscopy. Biophys. J. *73*, 2782–2790.

Petersen, J., Wilmann, P.G., Beddoe, T., Oakley, A.J., Devenish, R.J., Prescott, M., and Rossjohn, J. (2003). The 2.0-Å crystal structure of eqFP611, a far red fluorescent protein from the sea anemone *Entacmaea quadricolor*. J. Biol. Chem. *278*, 44626–44631.

Prasher, D.C., Eckenrode, V.K., Ward, W.W., Prendergast, F.G., and Cormier, M.J. (1992). Primary structure of the *Aeqourea victoria* green fluorescent protein. Gene *111*, 229–233.

Prescott, M., Ling, M., Beddoe, T., Oakley, A.J., Dove, S., Hoegh-Guldberg, O., Devenish, R.J., and Rossjohn, J. (2003). The 2.2 Å crystal structure of a pocilloporin pigment reveals a nonplanar chromophore conformation. Structure *11*, 275–284.

Quillin, M.L., Anstrom, D.M., Shu, X., O'Leary, S., Kallio, K., Chudakov, D.M., and Remington, S.J. (2005). Kindling fluorescent protein from *Anemonia sulcata*: dark-state structure at 1.38 Å resolution. Biochemistry *44*, 5774–5787.

Remington, S.J., Wachter, R.M., Yarbrough, D.K., Branchaud, B., Anderson, D.C., Kallio, K., and Lukyanov, K.A. (2005). zFP538, a yellow-fluorescent protein from *Zoanthus*, contains a novel three-ring chromophore. Biochemistry *44*, 202–212.

Schenk, A., Ivanchenko, S., Röcker, C., Wiedenmann, J., and Nienhaus, G.U. (2004). Photodynamics of red fluorescent proteins studied by fluorescence correlation spectroscopy. Biophys. J. *86*, 384–394.

Schiebel, E., and Maekawa, H. (2004). Cdk1–Clb4 controls the interaction of astral microtubule plus ends with subdomains of the daughter cell cortex. Genes Dev. *18*, 1709–1724.

Shaner, N.C., Campbell, R.E., Steinbach, P.A., Giepmans, B.N., Palmer, A.E., and Tsien, R.Y. (2004). Improved monomeric red, orange and yellow fluorescent proteins derived from *Discosoma* sp. red fluorescent protein. Nat. Biotechnol. *22*, 1567–1572.

Shcherbo, D., Merzlyak, E.M., Chepurnykh, T.V., Fradkov, A.F., Ermakova, G.V., Solovieva, E.A., Lukyanov, K.A., Bogdanova, E.A., Zaraisky, A.G., Lukyanov, S., and Chudakov, D.M. (2007). Bright far-red fluorescent protein for whole-body imaging. Nat. Methods *4*, 741–746.

Shimomura, O., Johnson, F.H., and Saiga, Y. (1962). Extraction, purification and properties of aequorin, a bioluminescent protein from the luminous hydromedusan, Aequorea. J. Cell. Comp. Physiol. *59*, 223–239.

Shkrob, M.A., Yanushevich, Y.G., Chudakov, D.M., Gurskaya, N.G., Labas, Y.A., Poponov, S.Y., Mudrik, N.N., Lukyanov, S., and Lukyanov, K.A. (2006). Far-red fluorescent proteins evolved from a blue chromoprotein from *Actinia equina*. Biochem. J. *392*, 649–654.

Terskikh, A., Fradkov, A., Ermakova, G., Zaraisky, A., Tan, P., Kajava, A.V., Zhao, X., Lukyanov, S., Matz, M., Kim, S., et al. (2000). Fluorescent timer: protein that changes color with time. Science *290*, 1585–1588.

Turcic, K., Pettikiriarachchi, A., Battad, J., Wilmann, P.G., Rossjohn, J., Dove, S.G., Devenish, R.G., and Prescott, M. (2006). Amino acid substitutions around the chromophore of the chromoprotein Rtms5 influence polypeptide cleavage. Biochem. Biophys. Res. Commun. *340*, 1139–1143.

von Wichert, G., Jiang, G., Kostic, A., De Vos, K., Sap, J., and Sheetz, M.P. (2003). RPTP-α acts as a transducer of mechanical force on α_v/β_3-integrin-cytoskeleton linkages. J. Cell Biol. *161*, 143–153.

Wall, M.A., Socolich, M., and Ranganathan, R. (2000). The structural basis for red fluorescence in the tetrameric GFP homolog DsRed. Nat. Struct. Biol. *12*, 1133–1138.

Wang, L., Jackson, W.C., Steinbach, P.A., and Tsien, R.Y. (2004). Evolution of new nonantibody proteins via iterative somatic hypermutation. Proc. Natl. Acad. Sci. USA *101*, 16745–16749.

Ward, W.W. (1981). Properties of the coelenterate green-fluorescent proteins. In Bioluminescence and Chemiluminescence: Basic Chemistry and Analytical Applications, M. DeLuca and D.W. McElroy, eds. (New York: Academic Press), pp. 235–242.

Ward, W.W. (2005). Biochemical and physical properties of green fluorescent protein. In Green Fluorescent Protein: Properties, Applications and Protocols, Second Edition, M. Chalfie and S.R. Kain, eds. (Hoboken, NJ: Wiley and Sons), pp. 39–65.

Ward, W.W., and Cormier, M.J. (1979). An energy transfer protein in coelenterate bioluminescence: characterization of the Renilla green-fluorescent protein (GFP). J. Biol. Chem. *254*, 781–788.

Wiedenmann, J. (1997). Die Anwendung eines orange fluoreszierenden Proteins und weiterer farbiger Proteine und der zugehörenden Gene aus der Artengruppe *Anemonia sp. (sulcata)* Pennant, (Cnidaria, Anthozoa, Actinaria) in Gentechnologie und Molekularbiologie. Patent DE 197 18 640. Deutsches Patent- und Markenamt, 1–18.

Wiedenmann, J., and Nienhaus, G.U. (2006). Live-cell imaging with EosFP and other photoactivatable marker proteins of the GFP family. Expert Rev. Proteomics *3*, 361–374.

Wiedenmann, J., Elke, C., Spindler, K.-D., and Funke, W. (2000). Cracks in the β-can: fluorescent proteins from *Anemonia sulcata* (Anthozoa, Actinaria). Proc. Natl. Acad. Sci. USA *26*, 14091–14096.

Wiedenmann, J., Schenk, A., Röcker, C., Girod, A., Spindler, K.-D., and Nienhaus, G.U. (2002). A far-red fluorescent protein with fast maturation and reduced oligomerization tendency from *Entacmaea quadricolor* (Cnidaria, Anthozoa, Actinaria). Proc. Natl. Acad. Sci. USA *99*, 11646–11651.

Wiedenmann, J., Ivanchenko, S., Oswald, F., Schmitt, F., Röcker, C., Salih, A., Spindler, K.D., and Nienhaus, G.U. (2004). EosFP, a fluorescent marker protein with UV-inducible green-to-red fluorescence conversion. Proc. Natl. Acad. Sci. USA *101*, 15905–15910.

Wiedenmann, J., Vallone, B., Renzi, F., Nienhaus, K., Ivanchenko, S., Röcker, C., and Nienhaus, G.U. (2005). The red fluorescent protein eqFP611 and its genetically engineered dimeric variants. J. Biomed. Opt. *10*, 14003.

Wilmann, P.G., Petersen, J., Devenish, R.J., Prescott, M., and Rossjohn, J. (2005). Variations on the GFP chromophore: a polypeptide fragmentation within the chromophore revealed in the 2.1-Å crystal structure of a nonfluorescent chromoprotein from *Anemonia sulcata*. J. Biol. Chem. *280*, 2401–2404.

Yang, M., Jiang, P., Yamamoto, N., Li, L., Geller, J., Moossa, A.R., and Hoffman, R.M. (2004). Real-time whole-body imaging of an orthotopic metastatic prostate cancer model expressing red fluorescent protein. Prostate *62*, 374–379.

Yanushevich, Y.G., Staroverov, D.B., Savitsky, A.P., Fradkov, A.F., Gurskaya, N.G., Bulina, M.E., Lukyanov, K.A., and Lukyanov, S.A. (2002). A strategy for the generation of non-aggregating mutants of Anthozoa fluorescent proteins. FEBS Lett. *511*, 11–14.

Yarbrough, D., Wachter, R.M., Kallio, K., Matz, M.V., and Remington, S.J. (2001). Refined crystal structure of DsRed, a red fluorescent protein from coral, at 2.0-Å resolution. Proc. Natl. Acad. Sci. USA *98*, 462–467.